

**Swift chemical sputtering of amorphous hydrogenated carbon**

E. Salonen, K. Nordlund, and J. Keinonen

*Accelerator Laboratory, P.O. Box 43, University of Helsinki, FIN-00014 Helsinki, Finland*

C. H. Wu

*EFDA, Max-Planck-Institut für Plasmaphysik, D-85748 Garching bei München, Germany*

(Received 12 October 2000; published 27 April 2001)

Ion bombardment of carbon materials is known to cause erosion with energies far below the threshold energy of physical sputtering, as well as at temperatures below the threshold of thermal desorption. Generally regarded as chemical sputtering, this effect, and factors contributing to it, are not well understood. We use classical molecular-dynamics simulations, capable of realistically describing bond formation and breaking, to study amorphous hydrogenated carbon surfaces under low-energy hydrogen bombardment. We present a swift chemical sputtering mechanism which can explain the experimentally observed characteristics of erosion by low-energy ion irradiation. We also show how the difference in the surface hydrogen concentration and carbon coordination fractions at various temperatures affect the carbon sputtering yield.

DOI: 10.1103/PhysRevB.63.195415

PACS number(s): 79.20.Ap, 34.50.Dy, 61.80.Az, 82.20.Wt

**I. INTRODUCTION**

The wide range of applications of amorphous hydrogenated carbon (*a*-C:H) is due to its unique materials characteristics.<sup>1,2</sup> Since the deposition and growth conditions are known to determine the properties of amorphous carbon materials,<sup>3–5</sup> it is imperative to understand the intricate physics and chemistry of interactions between impinging ions and *a*-C:H surfaces. While there is a large amount of experimental *a*-C:H deposition and irradiation data at low ( $\sim 0.1$ – $100$  eV) energies, the atomic-scale surface processes remain obscure and poorly understood. For instance, carbon erosion from *a*-C:H by hydrogen bombardment is known to occur under low-energy ( $\sim 10$  eV) conditions where the transfer of kinetic energy from the ions by elastic collisions is far too small to lead to significant physical sputtering yields.<sup>6–8</sup> Speculative of some sort of a bond-breaking process, this low-energy erosion regime is often called ion-assisted chemical sputtering. On the other hand, the ion energies are too large for a description of the process as a conventional etching-type chemical reaction. This conclusion is supported by the observed isotope effect<sup>8</sup> on the erosion yield, which indicates that a kinetic effect must be present in these interactions.

Standard sputtering models describing the erosion of materials assume that the sample composition remains constant during the bombardment. This, in turn, implies that the erosion yield is independent of the ion flux. However, recent high-ion-flux experiments<sup>9</sup> with fusion devices have shown that a flux dependence of the sputtering yield at very high fluxes ( $10^{18}$ – $10^{20}$  ions/cm<sup>2</sup> s) exists. In these cases the erosion of carbon-based materials under hydrogen ion and neutral hydrogen bombardment has been shown to decrease by an order of magnitude as the flux is increased. Since the experimental means to study atomic-scale phenomena are pushed to the extreme at low-energy and high-flux conditions, theoretical studies are called for to provide insight into surface interactions of hydrogen ions impinging on carbon surfaces.

This paper is organized as follows. In Sec. II we will

briefly go through the general properties of amorphous hydrogenated carbon, and previous model studies of carbon erosion by high- and low-energy hydrogen bombardment. In Sec. III we will describe in detail the molecular-dynamics simulation method we employed in this work. The results of the simulations will be presented in Secs. IV–VI. The paper will conclude with Sec. VII, in which we will discuss the validity of our modeling and its implications on the use of amorphous carbon materials as radiation-resistant material. Some of the results have been published elsewhere,<sup>10,11</sup> but will be briefly recalled since they are necessary to understand the pertinent results in this paper.

For different types of erosion we use the following terminology. If the erosion is due to collisional processes, it is called physical sputtering or just sputtering. Erosion by energetic particles, due to a mechanism where chemical bonds and their breaking play a crucial role, is called chemical sputtering.<sup>12</sup> If the sputtering occurs by a particle breaking a chemical bond, but does not involve a chemical reaction, we call the process “swift chemical sputtering.” Furthermore, a process is called chemically enhanced or reduced if the sputtering yield is affected by changes in the substrate material composition. Our definitions follow those in Ref. 12, except that we introduced the term swift chemical sputtering to denote a special type of chemical sputtering.

**II. BACKGROUND****A. Amorphous hydrogenated carbon**

During the last decades, the interest in amorphous hydrogenated carbon materials has been rapidly growing. They combine properties of hydrocarbon polymers and pure carbon structures (diamond and graphite), resulting in hard and chemically inert compounds with high cohesive energies and good thermal conductivity, as well as optical transparency windows in the visible and infrared regions.<sup>1,2</sup> These properties have given rise to the use of *a*-C:H as a corrosion and friction resistant coating in various applications, such as magnetic and optical recording disks.

One of the most challenging applications, both scientifically and technically, is the use of carbon-based coatings as a protective surface for the first wall structures in tokamak fusion devices. Due to the low atomic number of carbon, atoms sputtered from carbon-based first wall structures lead to much lower *bremstrahlung* and recombination radiation in the plasma than those sputtered from higher-*Z* elements. Hydrogen, on the other hand, is already present in the plasma, and hence it does not compromise the effective atomic number of the plasma and contaminate it. However, two major drawbacks to the use of carbon as a first wall material are the relatively high erosion yield compared with high-*Z* materials, for example tungsten and molybdenum, leading to low lifetimes for the plasma-facing components, and the harmful tritium retention in the wall structures. Understanding the reactions taking place at the surface of a fusion plasma-facing material under high-flux bombardment by hydrogen and plasma impurities, and the development of optimal plasma-facing materials, are of the utmost importance for the development of commercially viable fusion reactors.

Pure carbon materials, such as carbon fiber composites and graphites, become amorphous and hydrogenated very quickly under bombardment by hydrogen ions and neutral atoms. Energetic hydrogen ions and neutral atoms impinging on graphite layer planes cause bridging and bending of the layer planes over each other,<sup>13</sup> and the formation of large  $sp^3$  clusters between the planes. However, since the structure is highly disordered, no exact geometric configuration can be given for *a*-C:H, and the material must be characterized in another way. Three of the most important characteristics of an *a*-C:H sample are the hydrogen content, the  $sp^3/sp^2$  bonding ratio, and the density of the sample. High-density, high  $sp^3$ , and low hydrogen concentration (up to 30 at. %) hydrocarbon films are generally referred to as diamondlike carbon films or hard *a*-C:H, whereas low-density and high hydrogen concentration ( $\sim 50$ – $70$  at. %) *a*-C:H films are usually referred to as polymers or soft *a*-C:H. Laboratory experiments for graphites exposed to keV  $H^+$  beams have revealed that the hydrogenation of carbon structures saturates to a H/C ratio of about 0.4 at 300 K (Refs. 14 and 15), which decreases at higher temperatures.<sup>15,16</sup> For polymers the H/C ratio can be as high as 1.0. The stationary ratio of hydrogenation depends on the rates of hydrogen bonding to carbon vs hydrogen extraction via C—H bond breaking and  $H_2$  formation by impinging ions, as well as thermal desorption, at a given flux and sample temperature. Thermal decomposition of *a*-C:H films results in an increased fraction of  $sp^2$ -bonded carbon, as the weaker  $sp^3$  bonds are more easily broken with increasing thermal energy.

The properties of *a*-C:H are highly dependent on the deposition and growth conditions. It is clear that understanding the fundamental factors contributing to the microstructure, as well as the chemical and physical surface reactions taking place during the fabrication, is crucial if certain film properties are to be met. While a number of quantum-mechanical studies on the structure of *a*-C:H have been conducted,<sup>17–19</sup> the surface reactions taking place under low-energy ion irradiation still remain poorly understood. From a

computational point of view, a good force model, which realistically describes the structure and energetics of *a*-C:H, is required. Also, in order to make it possible to model a large number of atoms, the force model should not be too computationally demanding.

### B. Model studies for carbon erosion from *a*-C:H

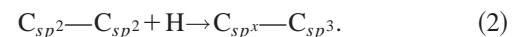
Carbon erosion from an *a*-C:H sample is usually considered to take place either as thermal desorption or physical sputtering. The thermal desorption of a sample requires only a sufficiently high temperature for the surface atom bonds to break. Although not energetic enough to directly kick atoms from their lattice sites, thermal ion irradiation can further increase the desorption rate of the sample by changing the bonding structure (via adsorption or abstraction) to a less inert configuration. Comprehensive studies by Horn *et al.* shared that the rate limiting step of thermal erosion of carbon from *a*-C:H is the breaking of C—CH<sub>3</sub> bonds.<sup>20</sup> The activation energy of this process is a 0.4-eV-wide Gaussian distribution with a mean value of 2.4 eV. The activation energy seems to be very low compared to a typical C—CH<sub>3</sub> bond energy (3.7 eV) in hydrocarbons. However, the release of methane is connected to the energy gain of the entire carbon-carbon network energy due to the  $sp^3 \rightarrow sp^2$  transition that takes place upon the radical release.

Thermal hydrogen irradiation of pure carbon or *a*-C:H leads to the bonding of H to the surface carbon atoms. In the case of pure carbon, a simultaneous irradiation or pre-irradiation by energetic ions<sup>21–24</sup> is usually required in order to produce bonding sites for the incoming thermal ions. Since carbon favors structures with threefold- or fourfold-coordinated carbon sites, it seems plausible that hydrogen atoms implanted into *a*-C:H bond to carbon atoms with coordinations of 3 or less. Thus the hydrogenation increases the amount of  $sp^3$ -bonded carbon atoms,



and also increases the thermal desorption of the sample.

Horn *et al.* presented a reaction scheme to explain the erosion of carbon from C:H films by thermal hydrogen.<sup>20</sup> Based on reactions they discovered in previous studies,<sup>25–27</sup> the scheme was explained to describe carbon erosion taking place via a —C—CH<sub>3</sub> bond split-off. The reason for this split-off is the relaxation of a neighboring intermediate  $sp^x$  carbon center. First, hydrogenation of an  $sp^2$  hybridized carbon center takes place due to the thermal H flux, leading to neighboring C—C network reconfiguration:



Provided a methyl radical is bonded to the  $sp^3$ -hybridized carbon center, the relaxation transition from  $sp^x$  to  $sp^2$  would lead to the release of the surface methyl radical. The activation energy given by Horn *et al.* for this reaction scheme was 1.6 eV, which is in good agreement with previous experimental studies.<sup>28</sup> Since one of the factors contributing strongly to the reaction scheme is the impinging hydrogen flux, the results indicate that the temperature range

where the erosion by thermal ions takes place will shift to higher temperatures at higher fluxes.<sup>20</sup> Although the authors correctly stated that they did not include in their model all reactions which can take place at C:H surfaces, the model did well reproduce the experimentally observed carbon desorption yields by thermal ions, as well as the transition from  $sp^3$  dominance to  $sp^2$  dominance in C:H films.

In the low-energy regime sputtering has been observed to take place under conditions where the transfer of kinetic energy by elastic collisions to sample atoms is far too low to lead to appreciable physical sputtering yields. For instance, erosion of carbon atoms and small molecules from hydrocarbon surfaces by  $\sim 10$ -eV hydrogen ions and neutrals is known to occur at yields orders of magnitude higher than expected for physical sputtering.<sup>6-8</sup> The low-energy erosion regime is frequently assumed to be due to some sort of bond-breaking mechanism. There have been modeling<sup>7,33</sup> and experimental attempts<sup>8,34</sup> to determine a threshold energy for this effect, but none has been found for ion energies  $\geq 10$  eV. A true understanding of how the sputtering actually occurs, as well as of the factors contributing to it, has been missing.

Physical sputtering and sputtering caused by electronic excitation are generally considered as the only types of erosion *directly*<sup>29</sup> caused by the bombarding ions.<sup>30,31</sup> In the present case, we do not consider it meaningful to consider the processes as electronic sputtering, as the electronic stopping power is not a well-defined concept for  $\sim 10$ -eV ions. Furthermore, although the bond-breaking processes found here are somewhat similar to some processes believed to be induced by electronic excitations during electronic sputtering,<sup>32</sup> we discuss our results in terms of elastic collisions and chemical reactions, as is commonly done in the field.

Based on previous analytic models, Roth and García-Rosales developed an analytical expression for the chemical erosion of carbon by hydrogen.<sup>7</sup> The goal was to present a model which would allow extrapolation of carbon erosion to the fluxes and energies relevant for fusion device divertor operation. The model describes physical sputtering and chemical erosion by high- and thermal-energy hydrogen, respectively, as well as enhancement of the chemical erosion due to formation of active sites for hydrogen bonding by the high-energy ions. The model also includes a factor which takes into account the "kinetic emission of weakly bound  $sp^3$   $CH_x$  species on the surface," namely, a chemical sputtering mechanism. This was included since it had been well established that carbon erosion under low-energy hydrogen irradiation took place at temperatures below the threshold temperature of 400 K of the model of Horn *et al.* Furthermore, while Horn *et al.*'s model did predict experimentally observed methane yields for thermal ion irradiation, it did not give a satisfying explanation for the observed yields of larger hydrocarbons, as there is no damage production mechanism to give rise to these hydrocarbon chains dangling at the surface. This indicates that the model cannot be applied for the case of  $\geq 1$ -eV ion bombardment.

The erosion yields of the unknown surface erosion mechanism also showed a clear isotope effect, which indi-

cated a kinetic mechanism. The exact details of this mechanism were not understood, but it was assumed to be an analogy of physical sputtering with a threshold energy close to the surface  $CH_x$  species binding energies. Since the concentration of  $sp^3$ -bonded carbon sites would decrease with increasing temperature, the kinetic hydrocarbon emission yield was also expected to decrease. Since at the time there were no data available for carbon erosion at energies below 10 eV, the model could only give extrapolations to this energy range.

It was observed experimentally that the peak temperature for carbon erosion increases with hydrogen flux up to a limiting value of  $\sim 950$  K (Refs. 35 and 36). The authors proposed that at temperatures above 900 K annealing and graphitization would suppress the methane production, and thus the carbon yield would consequently decrease at higher fluxes. However, this does not explain why carbon erosion would decrease at room temperature with increasing flux, which has been the case in experiments<sup>9</sup> conducted with the ASDEX Upgrade tokamak device.

A further attempt was made by Mech *et al.* to develop a self-consistent model<sup>33</sup> that takes into account the processes described above as well as some new ones, including the breaking of C=C double bonds by energetic hydrogen, and consequently producing  $sp^3$  and  $sp^x$  carbon sites. The best fits presented by the authors show an excellent agreement with experimental results, except at energies below  $\sim 25$  eV and at temperatures higher than  $\sim 800$  K. The authors concluded that there might be an additional low-energy process which is not included in the model. The kinetic ejection of the surface methyl groups was predicted to peak at energies between 30 and 50 eV by the model, and was concluded to be the dominant erosion mechanism at room temperature.

Finally, various mechanisms of low-energy chemical sputtering have previously been studied by molecular dynamics. Garrison and co-workers examined the sputtering and etching of silicon by fluorine and chlorine, giving detailed descriptions of the chemistry involved in the etching processes.<sup>37-39</sup> They described in detail a mechanism of chemical sputtering where an incoming F atom erodes an unsaturated  $SiF_3$  species from a silicon surface. The incident atom interacts with the F atoms bonded to the Si atom, changing their geometrical configuration from an  $sp^3$  tetrahedral configuration to a more planar form. The erosion follows from a nucleophilic substitution of the Si atom, where bonding to the incoming F atom leads to a stretching and eventually a breaking of the Si—Si bond that binds the  $SiF_3$  radical to the surface. Studies by Barone and Graves<sup>40,41</sup> on silicon sputtering by fluorine and chlorine by argon showed that a change of the surface composition at high fluxes can affect the sputtering yield.

To conclude this brief review of work in the field, we wish to emphasize that several authors found that chemical sputtering mechanisms of carbon are not well understood. Analytical models assume an effect that is present at very low energies and at temperatures below the threshold temperature of thermal desorption. Although previous

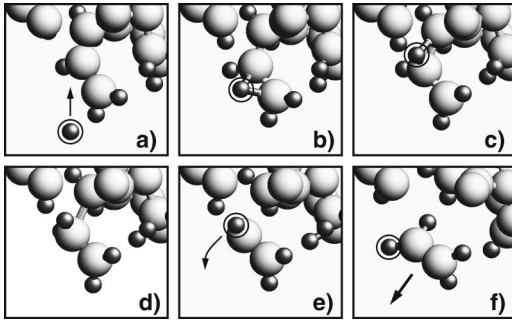


FIG. 1. Illustration of a  $C_2T_4$  radical erosion. The eroded species are determined by the length of the hydrocarbon chain above the broken C—C bond. In this particular case the ion (circled) impacts on the upper carbon atom forming the bond, and very efficiently enhances the bond breaking.

molecular-dynamics simulations presented some chemical sputtering mechanisms, these are not, however, applicable in this case.

### C. Carbon-carbon bond-breaking mechanism

In an earlier study we investigated the low-energy sputtering of  $a$ -C:H under low-energy hydrogen bombardment using molecular-dynamics computer simulations.<sup>11</sup> The simulation method was similar to the one used in this paper, and will be presented in Sec. III. We observed carbon erosion to take place in our simulations very quickly ( $\sim 100$ – $500$  fs). Since the incident ion energies were not large enough to cause physical sputtering, a chemical effect was expected. A thorough study of tens of bombardment events leading to carbon erosion showed a mechanism which we call *swift chemical sputtering*, since the process is chemical in nature but takes place rapidly. While the carbon erosion took place during the first 500 fs or so, the actual carbon-carbon bond breaking that eventually led to the erosion, could occur only a few tens of femtoseconds after the start of the simulation.

Since hydrogen is monovalent, it is the breaking of the C—C bonds that leads to carbon erosion from the sample. The chemical sputtering mechanism in our simulations was the breaking of those bonds by the impinging ion (Fig. 1). The fast ions attacked the region between two bonded carbon atoms. As the distance between the carbon atoms and the hydrogen atom at that point was less than  $0.75 \text{ \AA}$ , the repulsive part of the hydrogen-carbon potential energy function gave a significant increase to the potential energy of the carbon atoms forming the bond. It is this increase that made the bond breaking possible. The carbon atoms were pushed apart very quickly from each other, and the carbon network did not have time to relax to a new equilibrium bonding configuration. The repulsion eventually led to terminal separation, the distance of the two carbon atoms being larger than the  $2.0\text{-\AA}$  carbon-carbon cutoff radius of the Brenner potential, and the carbon-carbon bond was broken. The C—C separation could be further enhanced by collisions between the incident ion and the carbon atoms taking part in the bond-breaking process. In those cases momentum was transferred from the ion to the bulk carbon network atoms, and the C—C separation

occurred faster. Hydrocarbon species that were no longer bound to the bulk left the sample surface, along with any hydrogen atoms bonded to them.

Analysis of the energetics of this process showed that during the bond-breaking process the carbon-carbon potential energy is increased approximately by 4 eV, which is comparable to typical carbon-carbon  $sp^3$  and  $sp^2$  bond energies of 3.7 and 4.9 eV, respectively. Since the breaking of a carbon bond will lead to a reconfiguration of the neighboring carbon bonds, the energy needed to break the bond is likely to be somewhat lower than the bond strengths, as in the case of thermal desorption discussed earlier.

Simulations using cells with varying surface structures showed considerable differences in the amount of eroded carbon. Since the requirement for carbon erosion to occur is the breaking of all the C—C bonds binding an atom to the bulk, the probability for an atom to erode by the swift mechanism is determined by the number of carbon bonds the atom has. A carbon atom with only one or two C—C bonds erodes more easily than one with several C—C bonds. As the ions have very low energies and a single bond-breaking process consumes an energy of several eV (in addition to the energy lost in collisions with the surface atoms), carbon atoms with multiple bonds are not likely to erode by several, consecutive bond-breaking processes.

Thus, in most of the cases the carbon erosion was due to a single C—C bond rupture, and the determining factor for the nature of the eroded hydrocarbon species was the depth of the broken carbon-carbon bond. The dangling carbon chain at the surface, above the broken bond, was no longer bound to the bulk, and was eroded by the kinetic energy transferred in the bond-breaking process. It should also be mentioned that the incident ion did not always bond to the eroded hydrocarbon after the bond-breaking process, but would sometimes bond to the surface carbon instead.

## III. MOLECULAR-DYNAMICS SIMULATION METHOD

In molecular dynamics (MD) simulations the movement of particles (e.g., atoms, molecules, and nanoclusters) is simulated by deriving the force affecting the particles from some classical potential energy function, and numerically solving the equations of motion. This procedure is repeated in consecutive time steps. The choice for the length of these time steps in MD simulations is very important. Longer time steps can lead to an unphysical behavior of the system, such as a spontaneous cooling or heating of the simulation cell, caused by too abrupt changes of the atom positions. Shorter time steps, on the other hand, give a more realistic description of the system, but make the modeling of lengthier processes harder. Since the length of the time steps is usually of the order of  $\sim 0.01$ – $1$  fs, the modeled processes are limited to a few hundred nanoseconds.

If the maximum velocity  $\max(v)$  of the atoms changes significantly in time, it is possible to use a time-dependent length of the time step to speed up the simulation runs. For each new time step  $n$  the length of the time step  $\delta t_n$  is calculated from<sup>42</sup>

$$\delta t_n = \min\left(\frac{k_t}{\max(v_{n-1})}, \frac{E_t}{F_i v^{(i)}}, 1.1 \delta t_{n-1}\right), \quad (3)$$

where  $\max(v_{n-1})$  is the maximum velocity of the atoms in the cell, calculated for the previous time step, and  $k_t$  is the maximum displacement of a single atom per time step and is usually of the order of 0.1 Å. In the next term the constant  $E_t$  is approximately 300 eV,  $F_i$  is the total interatomic force affecting the atom  $i$ , and  $v^{(i)}$  the velocity of that particular atom.

The modeling in this paper was conducted with the HPCARCAS simulation code developed by Nordlund at the Accelerator Laboratory. The equations of motion are solved using a fifth-order Gear algorithm,<sup>43</sup> which is a predictor-corrector-type algorithm.<sup>44</sup> The temperature and pressure are controlled in our simulations by using the scaling methods of Berendsen *et al.*<sup>45</sup>

### A. Brenner-Beardmore empirical potential

For the potential-energy function in the modeling we chose the empirical Brenner-Beardmore hydrocarbon potential,<sup>46,47</sup> which is based on Abell-Tersoff formalism for covalent bonding.<sup>48,49</sup> Although the preceding Tersoff-type potentials reproduce a number of essential properties of diatomic and solid-state structures for carbon,<sup>50,51</sup> silicon,<sup>49</sup> and germanium,<sup>52</sup> problems with hydrocarbons arise for conjugated bonding and radical binding, for which the potential gives bonding energies that are too high. These issues are clearly extremely important when studying the interactions taking place at  $a$ -C:H surfaces, where the nature of the C:H bonding structure is heterogenous.

Brenner modified the standard Tersoff potential by introducing a highly parametrized bond-order function. The parameters were fit using a large number of experimental data on carbon and simple hydrocarbon molecules. The bond-order function essentially takes nonlocal effects into consideration, and correctly determines the conjugation state of carbon bonding configurations. Two parameter sets were originally published. The first parameter set gives a better description of carbon-carbon bond lengths, while the second one produces more accurate values for stretching force constants. Since we wanted to simulate hydrogen ion impacts on sample atoms, causing abrupt momentum transfers, we chose the second parameter set. Beardmore and Smith later combined the formulations of Tersoff<sup>52</sup> (Si—C), Brenner (C—H), and Murty and Atwater<sup>53</sup> (Si—H) to a hybrid potential for Si—C—H systems.<sup>47</sup>

The Brenner potential has a reasonably realistic description of pure carbon and hydrocarbon molecule structures, as well as the chemistry involved (bond forming and breaking), while not being computationally too intensive. Hence it has been used for various studies of carbon and hydrocarbon interactions.<sup>47,54–56</sup> The model does not incorporate electronic stopping, but in the energy range ( $\sim 1$ –35 eV) of this investigation it is not clear how the electronic stopping should be treated.

In order to find out whether the Brenner potential was suitable for simulating  $a$ -C:H bombardment, a number of

tests was done before starting the actual simulation runs. Since there is no single, unique  $a$ -C:H phase, there is also not a well-defined set of experimental microstructure data which could be used directly to test the applicability of the potential. Thus we chose to compare  $a$ -C:H structures produced by the Brenner potential with quantum-mechanical calculations. Galli *et al.* studied the microstructure of  $a$ -C:H with computer simulations based on density-functional theory.<sup>19</sup> An excellent agreement with experimentally measured fractions for threefold- and fourfold-coordinated carbon centers was observed at a fixed density and hydrogen content.

We created a bulk cell with properties matching the quantum-mechanical MD cell as closely as possible. Our test cell was manufactured with the method described in detail below (Sec. III B). The number of atoms in our cell was increased to 500 from 76 used in the quantum-mechanical MD cell. However, preparing the cell from a totally arbitrary initial configuration, by letting the potential-energy function used to find the minimum-energy structure, is a very delicate process. Thus the best correspondence we could obtain for a cell with a hydrogen content of 16 at.% was a density of  $\sim 2.7$  g/cm<sup>3</sup>, a bit higher than in the *ab initio* calculations. The obtained fractions for the threefold- and fourfold-coordinated carbon sites were 40% and 55%, in comparison with 55% and 41% reported by Galli *et al.*, respectively. A small number of twofold-coordinated carbon sites was also observed. As the increase in density with keeping the H/C ratio constant should result in a higher fraction of fourfold-coordinated carbon sites, the obtained fractions were reasonable. Quantum-mechanical structure calculations by Frauenheim *et al.*<sup>17</sup> also showed quantitatively similar tendencies.

We calculated carbon-carbon, carbon-hydrogen, and hydrogen-hydrogen radial distribution functions (RDF's) for our test cell which showed a reasonable agreement with the quantum-mechanical simulations, as can be seen in Fig. 2. Since the method of normalization of the radial distribution functions submitted by Galli *et al.* was not known to us, an exact comparison between the heights and widths of the peaks cannot be made.

In the carbon-carbon RDF ( $g_{CC}$ ) the first two peaks corresponding to the first- and second-neighbor distances appear at about the same distances (1.5 and 2.5 Å) in both radial distribution functions. In the carbon-hydrogen RDF the first peak is at 1.1 Å, which compares well with the calculated length of a C—H bond in simple hydrocarbons. A less intense second peak is at 2.2 Å in both pair correlation functions, but a smaller peak preceding that one is also seen at about 1.8 Å in our radial distribution function. The following peaks in the *ab initio* RDF were not observed in our simulations, and are likely statistical fluctuations caused by the small number of hydrogen atoms in the *ab initio* cell. In our hydrogen-hydrogen RDF there is a peak at about 0.75 Å which is due to hydrogen dimers that were not observed in the MD cell used by Galli *et al.* However, at higher temperatures H<sub>2</sub> dimers would most likely outgas from the sample or fracture due to C-H bonding. The number of hydrogen atoms in the quantum-mechanical cell was in our opinion very small (12 atoms) for any quantitative comparison of the hy-

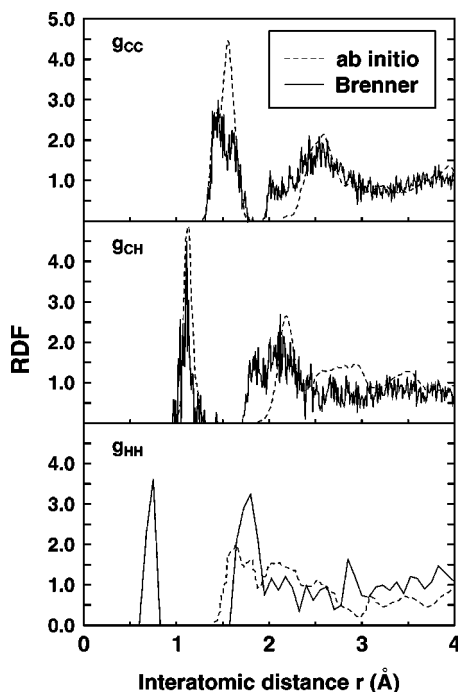


FIG. 2. Carbon-carbon, carbon-hydrogen, and hydrogen-hydrogen radial distribution functions (RDF) of the quantum-mechanical simulations and the Brenner potential test simulations

drogen distribution ( $g_{HH}$ ) in the cells. The large statistical uncertainties were also noted by the authors. Though inconvenient, this was of no large importance to us, as the main goal of these tests was to study the structure of the skeletal carbon network.

In simulations employing different pressure and temperature processing conditions, the cell properties (potential energies, densities, and atom coordinations) also behaved as expected on the basis of experimental data. The tests indicated that the Brenner potential gives a reasonably reliable description of  $a$ -C:H, and was considered to be suitable for simulations of ion bombardment. It should be mentioned that studies by Nordlund *et al.*<sup>51</sup> and Jäger and Albe<sup>57</sup> showed that the Tersoff-Brenner-type potentials do *not* give a good description of carbon phase transitions with the original potential cutoffs. Larger cutoffs, on the other hand, remove this problem. This modification, however, is not important in the present case, since there are no carbon phase transitions in our modeling.

### B. Simulation cells

Manufacturing an  $a$ -C:H cell suitable for the hydrogen bombardment simulations consisted of four different phases: (1) creating a random cell, (2) annealing the cell in order to find a stable structure, (3) obtaining the desired carbon coordination fractions, and (4) creating a stable surface. In the first simulations we used  $a$ -C:H cells having roughly the size of a  $15 \times 15 \times 15$ -Å<sup>3</sup> cube and consisting of 500 atoms. Cells of this size were adequately large for low-energy ( $E_{rms} \leq 10$  eV) hydrogen bombardment, but later we also used larger cells consisting of up to 2000 atoms for higher-energy cumulative simulation runs and in order to gain better statis-

tics. All hydrogen isotopes (H, D, and T) were used in the simulation cells and as impinging ions.

A random cell was created by first placing a number of carbon and hydrogen atoms at random in the cell, but setting a minimum distance between the atoms, corresponding approximately to the bond lengths between the elements in question, namely 1.5 Å for a C—C bond and 1.1 Å for a C—H bond.<sup>58</sup> For most of the cells we chose a H/C ratio of 0.4 in the cell to match the experimentally observed saturation value at 300 K (Refs. 14 and 15). However, simulation cells with different H/C ratios corresponding to the experimental saturation values at different temperatures were also manufactured in order to study the temperature dependence of the carbon erosion mechanisms.

Periodic boundaries were applied in the  $x$ ,  $y$ , and  $z$  directions, and atom movement in the random cell was simulated at temperatures between 4000 and 6000 K. After 5–10 ps the temperature was slowly ( $10^{13}$  K/s) quenched, letting the structure find a possible lowest-energy configuration as the temperature approached 0 K. This procedure was repeated until a clear minimum was found. A few more runs at lower (1000–3000 K) temperatures were done in order to overcome possible potential barriers toward even a lower-energy structure, until the potential energy no longer decreased.

The cell was then put under a very high constant pressure of  $\sim 10$ –1000 kbar for several picoseconds in order to achieve the desired  $sp^2$  and  $sp^3$  bonding fractions for the carbon atoms. The cell was then relaxed at zero pressure to form a stable cell again. It should be noted that there is no specific physical motivation for this particular method, but it gives a fairly good control over the atom coordinations. This final simulation phase, however, was not necessary for all the substrate cells, since picking reasonable initial values for the cell parameters, along with standard relaxation described above, resulted in many cases in satisfactory cell properties.

In order to form a surface, periodic boundary conditions were removed in the  $z$  direction, and the atoms within a distance of 2 Å from the bottom were held fixed. This was necessary, since we wanted to simulate  $a$ -C:H bulk instead of a thin film. Although this method is necessary, it is also clearly nonphysical. However, since there are no large cascades in low-energy bombardment such as that in the present work, very strong interactions never reach the fixed atoms. Finally, the cell was equilibrated in a thermal heat bath at 300 K for 50 ps after the opening of the surface, to remove any artificially broken bonds. During the equilibration a few atoms (mostly hydrogen) left the cell surfaces and were discarded from further simulations. Our simulation cell densities were approximately 2.4 g/cm<sup>3</sup> with threefold- and fourfold-coordinated carbon site fractions of 60–70% and 25–40%, respectively. A small number of onefold- and twofold-coordinated carbon sites were also seen at the surfaces. These properties are in good agreement with the density-functional calculations by Frauenheim *et al.*,<sup>17</sup> where the density and the fraction of fourfold-coordinated carbon sites for the most stable *bulk* cell with a hydrogen concentration of 33 at. % were 2.4 g/cm<sup>3</sup> and 41%, respectively.

### C. Hydrogen ion bombardment

Classical MD simulations cannot account for charge states of atoms. In the remainder of this paper we shall, however, use the term “ion” to denote the incoming atom regardless of its charge state, in order to make the following discussion easier to follow.

Simulating hydrogen bombardment was initiated by creating an ion outside an *a*-C:H cell, roughly 2 Å above the top surface atoms. Since the carbon-hydrogen cutoff radius of the Brenner potential is 1.8 Å, there was no interaction between the incident ion and the atoms of the cell at the start of the simulation. The incident ion energy was either selected randomly from the Maxwell-Boltzmann energy distribution for a rms energy (1 or 10 eV), or kept constant for each incident ion. The incident ion was assigned a velocity toward the surface, with a steep random off-normal angle between 0° and 20° and a random twist angle. The temperature was scaled to the selected substrate temperature within 2 Å from the borders in order to keep the substrate temperature constant, and to embed the energy brought into the cell by the impinging ion.

An impact on the surface too close to the cell borders could create unwanted artificial effects across the borders. Thus the center of the surface was always selected as the point of impact, and the cell was shifted a random distance in the *x* and *y* directions for each incident ion. This way the whole surface could be used as a target for the bombardment. Typical simulation runs consisted of 1000–6000 ion impacts. The impacts leading to sample erosion were later analyzed in detail.

We performed two main sets of bombardment simulation runs: *cumulative* and *noncumulative* hydrogen ion bombardment of *a*-C:H surfaces. In the cumulative runs an ion was shot on the surface and the cascade development was followed for 2–3 ps, depending on the kinetic energy of the ion. Hydrocarbon species sputtered from the surface were not included in the following simulations. Before shooting another ion on the surface the approximate location of the cell surface produced by the impact was calculated. The initial position of an ion was then modified so that the distance between the sample surface and the ion would be greater than the cutoff radius. The time interval between two consequent incident ions was long enough for the scaling at the borders to decrease the cell temperature back to the desired constant value, which in the case of cumulative bombardment was 300 K for all the simulation runs. The incident ion energy was chosen from the Maxwell-Boltzmann energy distribution.

In the noncumulative runs the same initial cell was used for each incident ion. The target cell was either a virgin (unsaturated) *a*-C:H cell, or a supersaturated (see below) cell produced in the cumulative runs. In these runs the cascade development was also followed for 2–3 ps. As well as running simulations where the incident ion energy was selected from the Maxwell-Boltzmann energy distribution, we studied the energy dependence of carbon erosion by running a series of simulations in which the kinetic energy was kept constant for each incident ion.

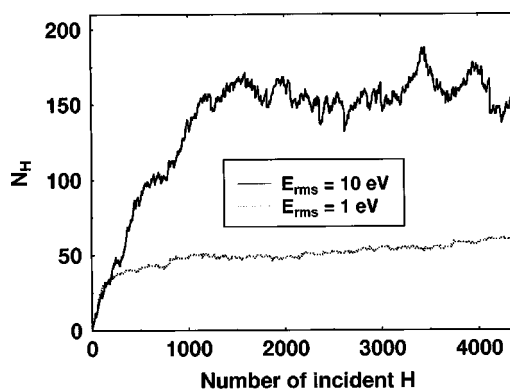


FIG. 3. Number of hydrogen atoms  $N_H$  in the cell in addition to the initial value at the start of the simulations for two cumulative hydrogen bombardment simulation runs. The fluctuations in the number of extra H in the cell were stronger for the  $E_{rms} = 10$  eV bombardment, where significant carbon erosion was also observed.

## IV. RESULTS OF THE CUMULATIVE SIMULATION RUNS

### A. $E_{rms} = 1$ eV bombardment

The effects of high fluences on the surface structure and carbon erosion yield were studied with cumulative simulations. The high rate of ion ( $E_{rms} = 1$  eV) incidence led to a strong hydrogen buildup on the cell surface during the first 500 incident ions; see Fig. 3. Between 500 and 1000 incident ions the hydrogen buildup slowed down, indicating a *supersaturation* of the hydrogen content in the cell. By supersaturation we mean here that the H/C ratio maintained by the high-flux H bombardment clearly exceeded the experimentally measured maximum H/C saturation ratio of 0.4 in bulk *a*-C:H. After 2000 ion impacts the hydrogen content in the cell increased only very slightly. Since the surface of the cell at the time was already highly coated with hydrogen (see Fig. 4), this increase was due to hydrogen-hydrogen replacement collisions of impinging ions driving hydrogen atoms into unsaturated regions deeper in the *a*-C:H cell. No carbon erosion was observed in these simulation runs.

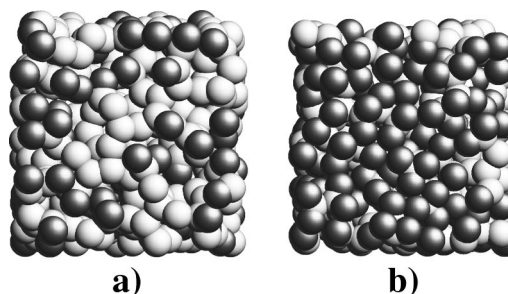


FIG. 4. Simulation cell surface seen from above at the start of the 1-eV hydrogen bombardment (a) and after 6000 incident ions (b). The dark spheres represent hydrogen atoms, and the light spheres represent carbon atoms. The supersaturated hydrogen coating leading to a decreased H-carbon-carbon bond collision cross section can be clearly seen. The atom sphere radii in the pictures are arbitrary.

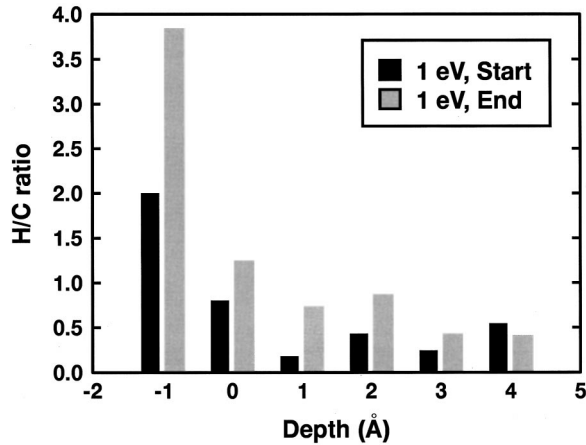


FIG. 5. H/C ratio near the simulation cell surface before (black bars) and after (grey bars) 1-eV cumulative bombardment. The initial cell surface is at 0.0 Å, the negative direction in the graph being outward from the bulk. The increased hydrogen concentration on the cell surfaces can be clearly seen. The high H/C ratio above the surface (at  $-1.0$  Å) is naturally due to the H-C bonding geometry of the carbon chains bound to the surfaces.

For an unsaturated surface the dominant hydrogen-surface interaction process was ion reflection from the surface. However, sputtering of hydrogen molecules (i.e., hydrogen capture) became more frequent with increasing hydrogen buildup on the surface. Since incident ion reflection does not affect the hydrogen concentration in the simulation cell, it is the hydrogen capture and hydrocarbon erosion that decrease the number of hydrogen atoms in the sample. Although higher at the end of the simulation runs, the probability of hydrogen capture still remained small enough for the high impinging hydrogen flux to produce and maintain a saturation of the hydrogen content on the surface. Figure 5 shows the H/C ratio in the cell before and after the simulation runs as a function of depth.

### B. $E_{rms} = 10$ eV bombardment

Since no carbon erosion was seen in the 1-eV simulations, we tested the hydrogen saturation effect at a higher rms energy of 10 eV. A similar increase of the hydrogen content in the cell was seen (Fig. 6). Since the simulation cell for higher-energy cumulative bombardment had to be much larger, obtaining a saturated hydrogen concentration at the surface required a higher number of impinging H ions as well. The rate of increase in the hydrogen concentration before obtaining the supersaturation value of H/C was nearly the same in both cases. However, the fluctuation of the hydrogen content at the surface was much stronger for the higher energy bombardment (cf. Fig. 3). The distribution of the incident ions remaining in the simulation cell after 5000 impacts as a function of depth is shown in Fig. 7. A root-mean-square energy of 10 eV was high enough to lead to carbon erosion. After 5000 incident ions, 181 carbon atoms out of the original 1433 had eroded from the surface, giving a carbon erosion yield of 0.04. The eroded carbon was mainly in  $\text{CH}_x$  ( $x=1, 2, 3,$  and  $4$ ) and  $\text{C}_2\text{H}_x$  ( $x=3, 4, 5,$  and  $6$ ) species, 58% and 31%, respectively.

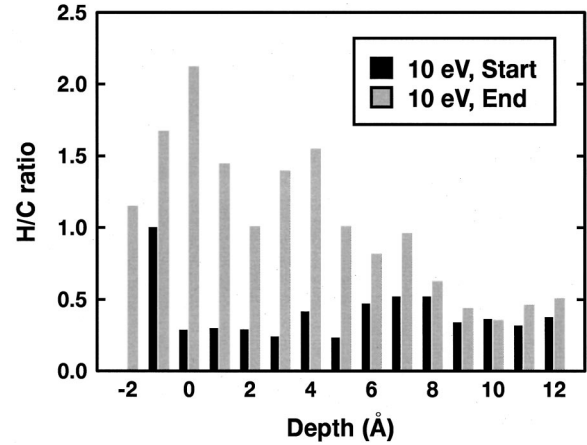


FIG. 6. As in Fig. 5, but for 10-eV ions.

## V. RESULTS OF THE NONCUMULATIVE SIMULATION RUNS

We studied the effects of the hydrogen concentration at the surface, incident ion energy, and the substrate temperature on the carbon erosion from the cell with noncumulative simulation runs. All of the three cases were studied independently of each other.

### A. Hydrogen shielding

The simulations studying the effect of the hydrogen concentration at the surface were run either with an unsaturated (virgin) *a*-C:T surface or a surface with a highly increased hydrogen concentration due to low-energy ion bombardment, that is, a surface formed after 1000 or more incident ions of  $E_{rms} = 1$  eV. We used tritium as cell atoms and ions, and the bombarding ions were assigned a rms energy of 10 eV. All the simulation runs were done at 300 K.

The high hydrogen concentration at the surface was observed to dramatically suppress carbon erosion from the

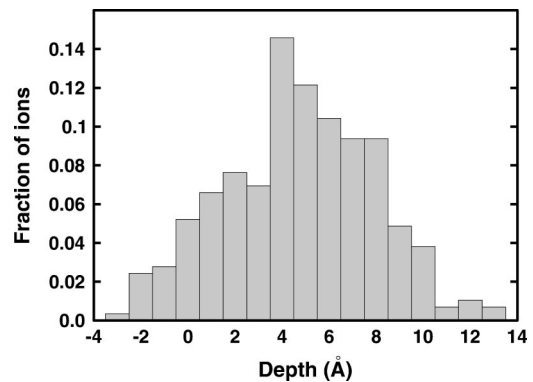


FIG. 7. Depth distribution of ions still remaining in the cell after 5000 incident ion impacts in the 10-eV noncumulative bombardment simulations. The negative direction is outward from the *a*-C:H bulk. 89% of the ions still reside under the original location of the surface, and 41% of the ions have penetrated 5 Å or deeper under the surface.

TABLE I. Fractions of the tritium erosion mechanisms for the noncumulative bombardment of an unsaturated and a supersaturated surface,  $E_{rms} = 10$  eV.  $Y_0^T$  and  $Y^T$  are the numbers of tritium eroded by the corresponding mechanism from the unsaturated and the saturated cell, respectively.

Erosion mechanism	Unsaturated surface	Supersaturated surface	$Y^T/Y_0^T$
Incident ion reflection	0.647	0.466	1.33
T <sub>2</sub> extraction	0.263	0.445	3.13
T atom sputtering	0.056	0.087	2.88
Hydrocarbon erosion	0.034	0.002	0.10

sample. With an unsaturated surface the carbon yield was  $(1.1 \pm 0.2) \times 10^{-2}$ , whereas with a supersaturated surface the carbon erosion yield had decreased by an order of magnitude, namely, to  $(1.6 \pm 0.8) \times 10^{-3}$ . This sharp drop of the carbon yield can be explained with a decreased carbon-carbon bond collision cross section. The impinging ions essentially lose the majority of their kinetic energy in collisions with the surface hydrogen before impacts with the carbon atoms. Thus the ions are not energetic enough to attack the region of a C—C bond, and are repelled by the potential barrier.

Carbon erosion from the virgin surface took place predominantly as CT<sub>x</sub> and C<sub>2</sub>T<sub>x</sub> species. A small number of single carbon atoms was also observed. The uncertainty in calculating the value of the carbon yield was quite high, but the high number of impinging ions gave us reasonable evidence of the order of magnitude. The results were later also confirmed with another independently manufactured virgin and supersaturated simulation cell pair.

Incident ion reflection was the most probable ion-surface processes, with both unsaturated and supersaturated surfaces. The tritium yield per incident ion with an unsaturated surface was  $\sim 0.5$ , of which about two-thirds was contributed by reflected ions and a little less than one-third by sputtered T<sub>2</sub> dimers. For a supersaturated surface the tritium yield was  $\sim 1.0$ . The probabilities of ion reflection and T<sub>2</sub> erosion were now roughly the same. Thus, the absolute value of both eroded T<sub>2</sub> and reflected ions was increased. More precise fractions for the tritium erosion are given in Table I.

In order to test the stability of the high hydrogen content at the surface, we simulated two different supersaturated cells at several temperatures between 300 and 2400 K for 1 ns (Ref. 10). The simulations were done without hydrogen bombardment, and thus focused on the thermal desorption (outgassing) of the surface hydrogen. However, since several outgassing mechanisms appeared to be present, and due to poor statistics at the lower temperatures, we were unable to extrapolate a statistically reliable outgassing rate for the surface hydrogen at 300 K.

### B. Incident ion energy dependence

The incident ion energy dependence of the carbon sputtering yield was studied with simulations where the same energy was assigned to each incident ion. The energy range used was 1–35 eV. The reason for this particular regime was that at energies lower than  $\sim 1$  eV no swift chemical sputtering was seen (see below). At energies  $\geq 35$  eV, on the

other hand, physical sputtering starts to dominate, and the simulation cell sizes used would not have been adequately large. The cell temperature was 300 K for all the simulation runs.

In the first simulation runs<sup>11</sup> we calculated the physical carbon sputtering yield and the carbon sputtering yield given by our MD simulations for an *a*-C:T cell bombarded by T ions. The physical sputtering yield was calculated using the TRIM program,<sup>59,60</sup> which takes into consideration only binary ion-atom interactions where the kinetic energy of the impinging ions is transferred to the substrate atoms in elastic collisions. Thus no chemical effects are present in the TRIM calculations. A comparison between our sputtering yields and those predicted by the TRIM code is shown in Fig. 8.

A small local maximum at energies close to 20 eV (cf. Fig. 8) indicates that at those energies, the bond-breaking mechanism has the highest probability. This maximum was also observed in several other simulation cells around 15–20 eV (see Fig. 9), although its strength varied from cell to cell, and it was pronounced only for T bombardment. This again shows that the results are quite sensitive to the bonding characteristics right at the surface. Since the impinging ions also experience non-bond-breaking collisions with surface hydrogen and carbon atoms, which extract even more energy from the ion, in most cases a kinetic energy of several eV above the threshold energy for the bond breaking is necessary.

By gradually lowering the incident ion energy in single impact simulations leading to carbon sputtering, a threshold

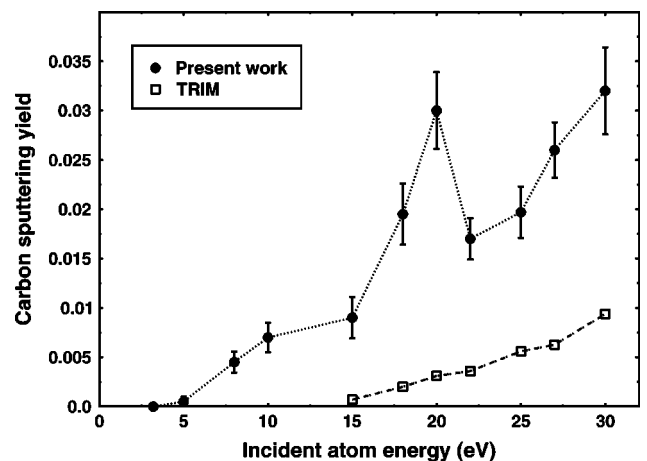


FIG. 8. Comparison of the carbon sputtering yield of our simulations of T impinging on *a*-C:T with TRIM simulations of physical sputtering. From Ref. 11.

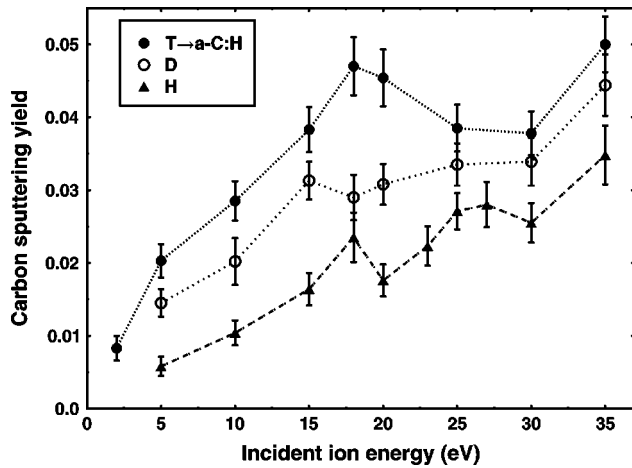


FIG. 9. Carbon sputtering yield for an  $a$ -C:H cell by proton, and deuterium and tritium ion noncumulative bombardment of  $a$ -C:H as a function of incident ion energy. The results show a clear isotope effect for the swift chemical sputtering.

energy was eventually found. No carbon sputtering was seen at ion energies below  $\sim 1.0$  eV for any of the three isotopes H, D, or T.

We also simulated monoenergetic bombardment of  $a$ -C:H by protons and deuterium and tritium ions in order to observe possible isotope effects. Figure 9 shows that the carbon erosion is notably higher in the case of heavier isotopes. This confirms that the swift chemical sputtering observed in our simulations is subject to kinetic effects and is not a purely chemical process. Considering the cases where the bond breaking is enhanced by the collisions between the incident ion and one or several surface carbon atoms taking part in the bond-breaking process, the existence of an isotope effect is easy to understand.

### C. Temperature-independent T/C ratio

The temperature dependence of the carbon erosion was first studied using a simulation cell with a constant T/C ratio

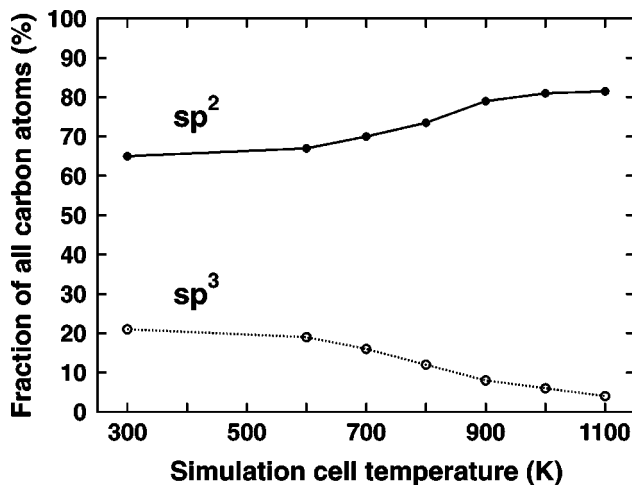


FIG. 10. Fractions of the threefold- and fourfold-coordinated carbon atoms in a constant T/C ratio simulation cell as a function of temperature.

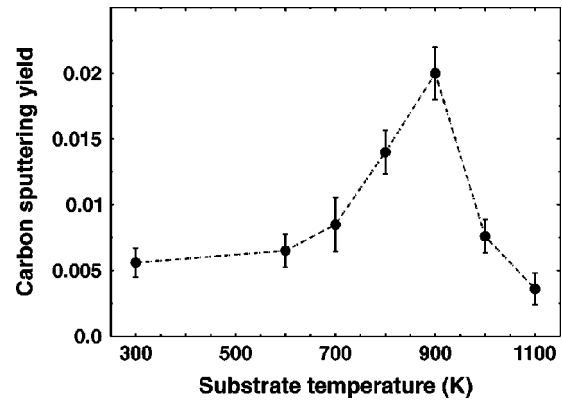


FIG. 11. Carbon sputtering yield as a function of temperature in noncumulative T bombardment simulations for a cell with temperature independent T/C ratio (0.4). A similar behavior was observed for other simulation cells. From Ref. 11.

(0.4). In the temperature range of our simulations, this corresponds roughly to the case where the sample is hydrogenated before heating.<sup>16</sup> The cells were heated very slowly for a MD simulation ( $10^{13}$  K/s) from 300 K to several temperatures between 600 and 1100 K, and then relaxed for 50 ps. Any atoms that left the sample surface during the heating were discarded. During the heating the fraction of threefold-coordinated carbon sites in the cell increased with increasing temperature, and the fraction of fourfold-coordinated carbon sites decreased (see Fig. 10). Since only a few hydrogen atoms left the surface during the heating, the concentration of hydrogen atoms in our cell remained practically constant at all temperatures. Thus an increase in the relative number of threefold-coordinated carbon centers meant a decrease of the total carbon coordination in the cell. Although the time scales used were too short for actual graphitization, the monotonic increase and decrease was present in all of our simulation cells, manufactured independently of each other. The ion bombardment simulations on these cells were noncumulative.

Figure 11 shows the typical temperature dependence for carbon erosion in our simulations. A clear maximum around 900 K can be seen. A temperature peak in the carbon erosion yield is typical for chemical sputtering,<sup>12</sup> which is another indication of the chemical nature of the carbon erosion mechanism we observed. Experimental values for the carbon erosion peak temperature  $T_m$  between 600 and 950 K were reported,<sup>7,8,61</sup> and the value of the peak temperature was shown to depend on the sample structure, graphitelike samples having the highest  $T_m$ . Since our simulation cells consist mostly of threefold-coordinated carbon sites, our results are in a reasonable agreement with the experiments.

The distributions of eroded hydrocarbon species at various temperatures did not have notable differences. The sputtered species were mainly small  $CT_x$  and  $C_2T_x$  hydrocarbons (Fig. 12). One larger  $C_5T_5$  species was observed to leave the surface, and did not fracture during the simulation time. However, the simulation time (2–3 ps) for a single impact was clearly too short to allow any conclusions on fragmentation or interaction between the sputtered species.

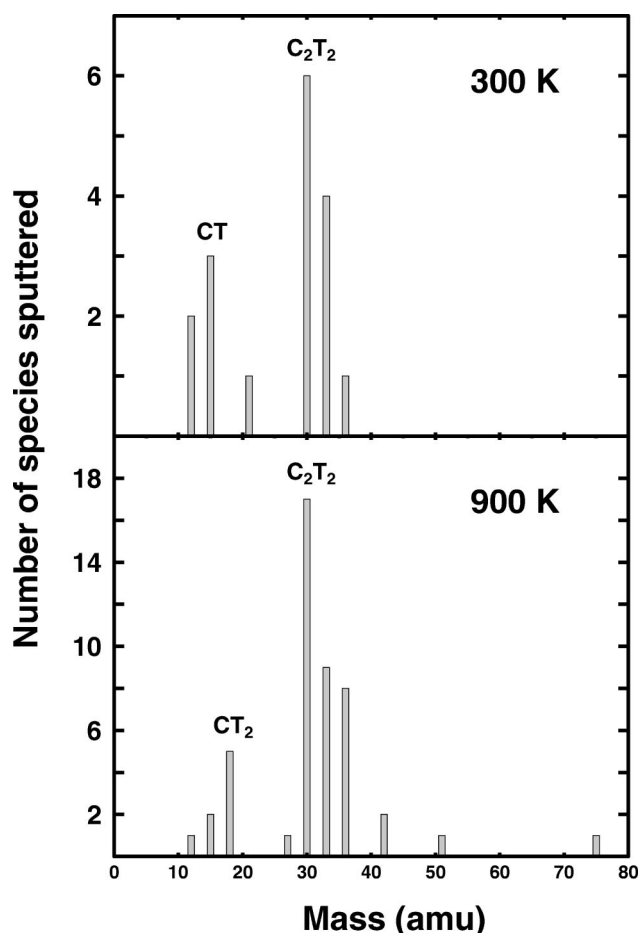


FIG. 12. Mass distributions of hydrocarbon species sputtered in constant T/C cell bombardment at 300 and 900 K. At both temperatures  $C_2T_2$  was the most abundant eroded species. However, as the simulations were noncumulative, the distribution was sensitive to the particular bonding configuration at the sample surface.

Considering the nature of our carbon erosion mechanism, the increase in the number of carbons eroded from the cell at higher temperatures is easy to understand. Decreasing the average carbon-carbon coordination led to a structure that was more prone to the swift erosion mechanism. But why does the carbon yield go down above 900 K? Simulations with very rapidly heated cells, where structural rearrangement had no time to take place, did not show an increase in the carbon erosion yield. This shows that, in the temperature range used, the effect of thermal vibrations is of secondary importance.

We analyzed the depth distributions for the eroded carbon atoms (Fig. 13). At temperatures between 300 and 900 K an approximately 4–5-Å-wide distribution was seen. Above 900 K, however, the distribution of the eroded carbon atoms shifted toward the surface. There is no reason to believe that the ions were unable to penetrate the surface as they had done at lower temperatures. This indicates that carbon atoms whose bonds had been broken deep below the surface rebounded, and did not leave the surface. This is somewhat unexpected, since an increase in temperature usually results in higher mobility of atoms in a bulk network. However, due

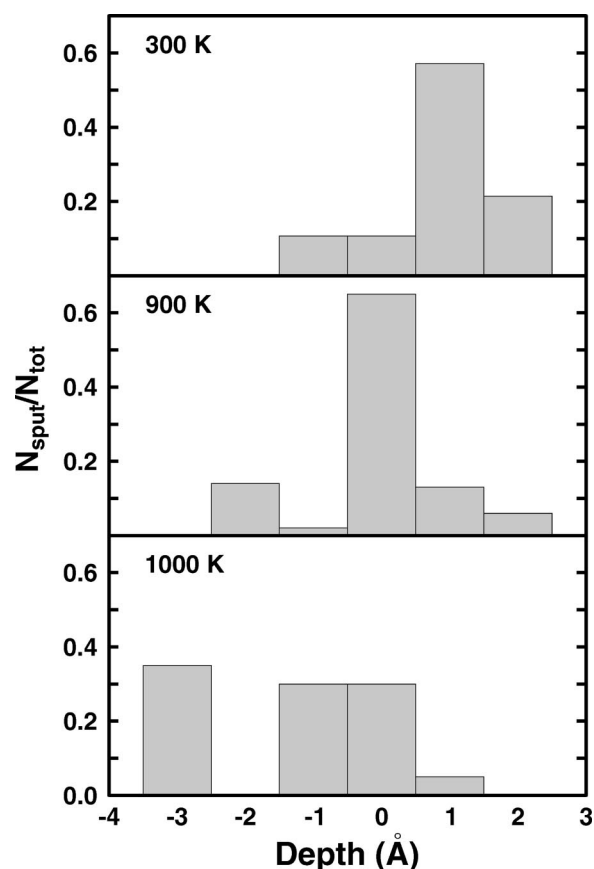


FIG. 13. Depth distribution of the eroded carbons for a T/C = 0.4 simulation cell under 10 eV bombardment at 300, 900, and 1000 K. The negative direction is outwards from the bulk, and the surface is approximately at 0.0 Å. The graphs show how the distribution shifts above the surface with increasing temperature.

to the heterogeneous nature of the bonding configuration in our cell, and the fact that the total carbon coordination decreases at higher temperatures, the free carbon atoms under the surface have a higher probability of encountering an unsaturated (coordination of three or less) carbon center while leaving the surface. It is then possible that the free carbon atoms rebound to the bulk network.

It should be noted that it was very hard to study possible rebonding. Among thousands of bombardment events, it is easy to study cases in which erosion does occur, but very difficult to recognize the cases where erosion *almost* occurs, namely, bond breaking and rebonding. The assumption was put to test with another type of simulation. We simulated a cell at various temperatures without any hydrogen bombardment. A single carbon atom bonded to the bulk network was given a velocity toward the surface with a random off-surface angle ( $0^\circ$ – $30^\circ$ ), corresponding to a certain kinetic energy. The lowest assigned kinetic energy was the total bond energy of all the C–C bonds of that particular carbon atom, and several tens of events were simulated in order to obtain good statistics. The kinetic energy was gradually raised in consecutive sets of simulation runs. The results showed that removing carbon atoms from the cell at a temperature above 900 K requires higher kinetic energies than at

900 K or below. These results support the idea of dynamic rebonding, but the reasons why the rebonding commences at these temperatures are not obvious, and should be studied with more precise methods.

#### D. Temperature-dependent T/C ratios

Simulation cells with temperature-dependent T/C ratios corresponded better to real cases where the hydrogen saturation concentrations are lower at higher temperatures due to diffusion, and consequently outgassing. We studied two cases in particular: (1) a sample that has been hydrogenated at low temperature (300 K) and then heated, and (2) a sample that has been hydrogenated at each temperature in question. The T/C ratios at different temperatures were chosen according to the experimental results in Refs. 15 and 16. Cell manufacturing was done with the same method described in detail in Sec. III.

Figure 14 shows that in both cases the decrease in the T/C ratio led to a decrease in the carbon erosion yield. In the first case the decrease was monotonic and no peak was observed. In the second case, on the other hand, a peak was observed around 700 K. Analogous to the case of a temperature-independent T/C ratio, this peak was due to the decrease of the average carbon-carbon coordination with increasing temperature, while the hydrogen concentration in the cell remained constant. At higher temperatures, as the T/C ratio decreased, the carbon erosion yield decreased like in the first temperature-dependent T/C case. This kind of temperature dependence corresponds to the behavior of the kinetic enhanced hydrocarbon emission used in the model of Roth and García-Rosales.

## VI. DISCUSSION

Our simulation results offer explanations for some poorly understood effects at carbon material surfaces. However, we wish to mention some points that should be taken into consideration when relating the simulation results to real processes.

#### A. Hydrogen shielding and its implications to high ion fluxes

Our cumulative simulation runs corresponded to a flux of  $\sim 10^{25}$  ions/cm<sup>2</sup>s, which is still orders of magnitude higher than the fluxes used in fusion devices. However, the fluxes corresponding to the highest hydrogen fluxes that have been used in fusion device experiments ( $\sim 10^{19}$  atoms/cm<sup>2</sup>s) would require time intervals of the order of microseconds with the method used. Although some methods for simulating times of the order of microseconds or even longer were recently developed,<sup>62,63</sup> these methods are quite specific and require a good knowledge of the local energy minima of the system, which is not, unfortunately, the case with *a*-C:H. Nevertheless, from our results we were able to give an upper limit for the desorption rate at 300 K. Since no hydrogen erosion was seen during outgassing simulation runs of 1 ns, the shielding effect should be possible, according to our modeling, with fluxes at least as low as  $\sim 10^{22}$  atoms/cm<sup>2</sup>s.

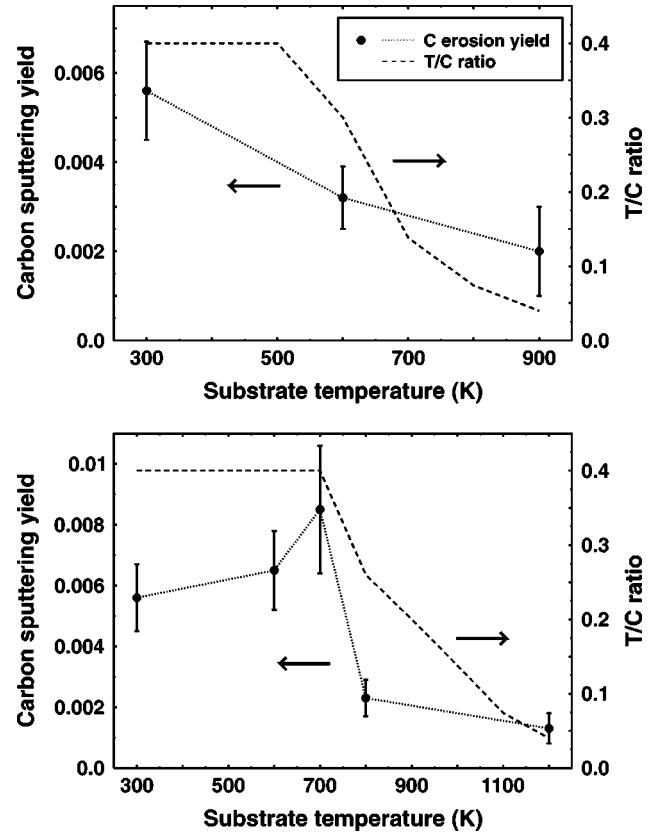


FIG. 14. Carbon sputtering yield as a function of temperature in noncumulative T bombardment simulations for substrate simulation cells with T/C ratios corresponding to experimentally observed hydrogen saturation values (Refs. 15 and 16). The upper figure corresponds to the case where the sample has been hydrogenated at a low temperature and then heated, whereas the lower figure shows the case where the sample has been hydrogenated at the respective temperature.

Here the crucial question is how stable the supersaturation is at the surface at 300 K. If the thermal desorption of the hydrogen atoms is slow enough, the hydrogen shielding effect could be obtained at lower fluxes than the low limit we estimated from our simulations. Thus finding statistically reliable outgassing rates of hydrogen from *a*-C:H surfaces at different temperatures is important. Also, in real processes, hydrogen *molecule* outgassing would most likely play a key role. Surface H-H attraction resulting in hydrogen molecule formation and erosion could very efficiently remove the hydrogen coating at the surface. Modeling the stability of the hydrogen coating requires long-range potential energy functions, such as the AIREBO (adaptive intermolecular reactive empirical bond-order),<sup>64</sup> as well as much longer time scales. This, however, is beyond the scope of the current work.

Whether the shielding effect we observed in our modeling is the key factor to explain the decrease of carbon erosion yield at high fluxes remains to be seen, as the real fluxes are orders of magnitude lower than the flux we used. If so, this effect can then be used to increase the lifetime of fusion device divertor plates, which experience extremely high-flux, low-energy hydrogen ion and atom bombardment. With suitable carbon material selection, the carbon erosion yields can

be modified to match the desired radiative cooling and plasma contamination by carbon. Also, since the impinging hydrogen is retained very near the surface, and the supersaturation increases the incident ion reflection, tritium retention in the first wall materials can be suppressed. This also requires that the mobility of the ions remaining in the bulk is hindered by a high H/C ratio already present in the material. As next generation fusion devices will be realized in the near future, more reliable experimental results can also be expected at higher fluxes.

### B. Low-energy chemical sputtering

The swift chemical sputtering mechanism in our modeling resembles an assumed surface erosion process, which in the literature is often called “kinetic emission of weakly bound surface hydrocarbons.” However, it should be noted that the bond breaking described above can take place at very low energies (just enough for the ion to overcome the repulsion of the C—C and to penetrate between the atoms), and no collisions are necessary for the erosion to take place. The threshold observed in our simulations ( $\sim 1.0$  eV) is in good agreement with previous analytical model extrapolations. We would also like to note that we have observed the same swift erosion mechanism in simulations of pure amorphous carbon and amorphous hydrogenated silicon carbide (*a*-SiC:H).<sup>65</sup>

As experimental methods for ion energies below 10 eV will presumably be realized in the near future, our modeling will be put to test and will offer a good point of comparison for experiments and simulations likewise. However, two points should be taken into account in these comparisons. First, contemporary experiments are done with dimers ( $\text{H}_2^+/\text{D}_2^+$ ) or trimers ( $\text{H}_3^+/\text{D}_3^+$ ), and the “single-ion energy” is taken as one-half (one-third) of the dimer (trimer). At low energies, however, bond energies play a crucial role, and it is not evident that the ion interactions with the surface are not modified by the presence of the other ion(s). Second, there was no surface relaxation in the cumulative high-flux bombardment simulations between two consecutive ions, aside from the short time during which the cell temperature decreased back to the desired value. This can affect the extrapolation to lower fluxes, as there would be more time for intermediate radical configurations to relax or passivate. Also, due to the method of cell manufacturing, we cannot state with *full* certainty that even the initial cell surface used for noncumulative simulations is fully relaxed. However, as the surface was given ample time to equilibrate, we do not believe that the results of the current work are strongly affected by that effect.

## VII. CONCLUSIONS

The present work demonstrates that molecular-dynamics modeling can be a very useful tool in studying and understanding atomic-scale surface effects, such as sputtering and thin-film growth. This is valid especially for amorphous surfaces, as an analytical study of these is extremely difficult. The results also demonstrate that standard sputtering models are not necessarily reliable at high fluxes, since they do not account for effects in which the relative surface atom concentrations change during the irradiation. Quantum-mechanical calculations of more accurate energetics, as well as the effect of the charge state of the incident atom on the swift chemical sputtering, are beyond the scope of the present study, but are under preparation as a next step to understand in more detail the effects studied.

In conclusion, we have shown that a high-flux, low-energy ( $E \leq 10$  eV) hydrogen bombardment of hard amorphous hydrogenated carbon results in a supersaturated hydrogen concentration at the immediate surface. This hydrogen coating very efficiently decreases the carbon sputtering yield from the sample. We have also described in detail how low-energy hydrogen ion bombardment at lower fluxes can lead to carbon sputtering yields much higher than those expected from physical sputtering. The carbon yield of this mechanism, which we call *swift chemical sputtering*, has been shown to decrease at higher temperatures, if the hydrogen concentrations in the cell are chosen to correspond to the experimental temperature-dependent saturation values. The temperature  $T_m$  corresponding to the highest erosion yield is determined by the temperature-dependent H/C ratios, and the carbon-carbon coordinations at respective temperatures. On the other hand, if the hydrogen concentration in the sample is kept constant at all temperatures, the carbon erosion by the swift erosion mechanism peaks at temperatures around 900 K.

## ACKNOWLEDGMENTS

We thank Professor D. W. Brenner and Dr. K. Beardmore for giving their implementations of the hydrocarbon potential to the authors' use. We would also like to thank Professor B. Garrison for useful discussions. The research was supported by TEKES under the FFUSION2 program, and the Academy of Finland under Project Nos. 35073 and 44215. Grants of computer time from the Center for Scientific Computing in Espoo, Finland, are gratefully acknowledged.

<sup>1</sup>J.C. Angus and C.C. Hayman, *Science* **241**, 913 (1988).

<sup>2</sup>W. Jacob, *Thin Solid Films* **326**, 1 (1998), and references therein.

<sup>3</sup>W.S. Bacsa, J.S. Lannin, D.L. Pappas, and J.J. Cuomo, *Phys. Rev. B* **47**, R10 931 (1993).

<sup>4</sup>S. Sattel, J. Robertson, and Ehrhardt, *J. Appl. Phys.* **82**, 4566 (1997).

<sup>5</sup>D. Bourgoin, S. Turgeon, and G.G. Ross, *Thin Solid Films* **357**, 246 (1999).

<sup>6</sup>A. Annen and W. Jacob, *Appl. Phys. Lett.* **71**, 1326 (1997).

<sup>7</sup>J. Roth and C. Garcia-Rosales, *Nucl. Fusion* **36**, 1647 (1996), and references therein.

<sup>8</sup>B.V. Mech, A.A. Haasz, and J.W. Davis, *J. Nucl. Mater.* **255**, 153

- (1998).
- <sup>9</sup>A. Kallenbach, A. Thoma, A. Bard, K. Behringer, K. Schmidtman, M. Weinlich, and the ASDEX upgrade team, *Nucl. Fusion* **38**, 1097 (1998).
  - <sup>10</sup>E. Salonen, K. Nordlund, J. Tarus, T. Ahlgren, J. Keinonen, and C.H. Wu, *Phys. Rev. B* **60**, R14005 (1999).
  - <sup>11</sup>E. Salonen, K. Nordlund, J. Keinonen, and C.H. Wu, *Europhys. Lett.* **52**, 504 (2000).
  - <sup>12</sup>J. Roth, in *Sputtering by Particle Bombardment*, edited by R. Behrisch (Springer, Berlin, 1981), Vol. I, pp. 91–146.
  - <sup>13</sup>T. Tanabe, *Phys. Scr.* **T64**, 7 (1996).
  - <sup>14</sup>J. Roth, B.M.U. Scherzer, R.S. Blewer, D.K. Brice, S.T. Picraux, and W.R. Wampler, *J. Nucl. Mater.* **93&94**, 601 (1980).
  - <sup>15</sup>B.L. Doyle, W.R. Wampler, and D.K. Brice, *J. Nucl. Mater.* **103&104**, 513 (1981).
  - <sup>16</sup>G. Federici and C.H. Wu, *J. Nucl. Mater.* **207**, 62 (1993), and references therein.
  - <sup>17</sup>T. Frauenheim, P. Blaudeck, U. Stephan, and G. Jungnickel, *Phys. Rev. B* **48**, 4823 (1993).
  - <sup>18</sup>G. Jungnickel, T. Frauenheim, D. Porezag, P. Blaudeck, U. Stephan, and R.J. Newport, *Phys. Rev. B* **50**, 6709 (1994).
  - <sup>19</sup>G. Galli, S. Iarlori, and O. Martini, *Phys. Rev. B* **49**, 7060 (1994).
  - <sup>20</sup>A. Horn, A. Schenk, J. Biener, B. Winter, C. Lutterloh, M. Wittman, and J. Küppers, *Chem. Phys. Lett.* **231**, 193 (1994).
  - <sup>21</sup>E. Vietzke, K. Flaskamp, and V. Philipps, *J. Nucl. Mater.* **111-112**, 763 (1982).
  - <sup>22</sup>A.A. Haasz, O. Auciello, P.C. Stangeby, and I.S. Youle, *J. Nucl. Mater.* **128-129**, 593 (1984).
  - <sup>23</sup>E. Vietzke, V. Philipps, and K. Flaskamp, *J. Nucl. Mater.* **162-164**, 898 (1989).
  - <sup>24</sup>E. Vietzke and A.A. Haasz, in *Physical Processes of the Interaction of Fusion Plasmas with Solids*, edited by W.O. Hofer and J. Roth (Academic Press, San Diego, 1996), Chap. 4.
  - <sup>25</sup>J. Biener, U.A. Schubert, A. Schenk, B. Winter, C. Lutterloh, and J. Küppers, *Adv. Mater.* **5**, 639 (1993).
  - <sup>26</sup>J. Biener, U.A. Schubert, A. Schenk, B. Winter, C. Lutterloh, and J. Küppers, *J. Chem. Phys.* **99**, 3125 (1993).
  - <sup>27</sup>C. Lutterloh, A. Schenk, B. Winter, J. Biener, U.A. Schubert, and J. Küppers, *Surf. Sci.* **316**, L1039 (1994).
  - <sup>28</sup>E. Villa, J.A. Dagata, J. Horwitz, D. Squire, and M.C. Lin, *J. Vac. Sci. Technol. A* **8**, 3237 (1990).
  - <sup>29</sup>The erosion caused by thermal ions takes place due to changes in the bonding configuration, as discussed above, and is not directly caused by the impinging ions.
  - <sup>30</sup>*Sputtering by Particle Bombardment I*, edited by R. Behrisch (Springer, Berlin, 1981).
  - <sup>31</sup>P. Sigmund, *Mat. Fys. Medd. K. Dan. Vidensk. Selsk.* **43**, 7 (1993).
  - <sup>32</sup>R.E. Johnson and J. Schou, *Mat. Fys. Medd. K. Dan. Vidensk. Selsk.* **43**, 403 (1993).
  - <sup>33</sup>B.V. Mech, A.A. Haasz, and J.W. Davis, *J. Appl. Phys.* **84**, 1655 (1998).
  - <sup>34</sup>C. García-Rosales, and J. Roth, *J. Nucl. Mater.* **196-198**, 573 (1992).
  - <sup>35</sup>J. Roth, J. Bohdanský, and K.L. Wilson, *J. Nucl. Mater.* **111-112**, 775 (1982).
  - <sup>36</sup>D.M. Goebel, J. Bohdanský, R.W. Conn, Y. Hirooka, W.K. Leung, R.E. Nygren, and G.R. Tynan, *Fusion Technol.* **15**, 102 (1989).
  - <sup>37</sup>B.J. Garrison and W.A. Goddard III, *Phys. Rev. B* **36**, 9805 (1987).
  - <sup>38</sup>T.A. Schoolcraft and B.J. Garrison, *J. Am. Chem. Soc.* **113**, 8221 (1991).
  - <sup>39</sup>H. Feil, J. Dieleman, and B.J. Garrison, *J. Appl. Phys.* **74**, 1303 (1993).
  - <sup>40</sup>M.E. Barone and D.B. Graves, *J. Appl. Phys.* **78**, 6604 (1995).
  - <sup>41</sup>M.E. Barone and D.B. Graves, *J. Appl. Phys.* **77**, 1263 (1995).
  - <sup>42</sup>K. Nordlund, *Comput. Mater. Sci.* **3**, 448 (1995).
  - <sup>43</sup>G. Gear, *Numerical Initial Value Problems in Ordinary Differential Equations* (Prentice-Hall, Englewood Cliffs, NJ, 1971).
  - <sup>44</sup>W.H. Press, S.A. Teukolsky, W.T. Vetterling, and B.P. Flannery, *Numerical Recipes in C; The Art of Scientific Computing*, 2nd ed. (Cambridge University Press, New York, 1995).
  - <sup>45</sup>H.J.C. Berendsen, J.P.M. Postma, W.F. van Gunsteren, A. Dinola, and J.R. Haak, *J. Chem. Phys.* **81**, 3684 (1984).
  - <sup>46</sup>D.W. Brenner, *Phys. Rev. B* **42**, 9458 (1990).
  - <sup>47</sup>K. Beardmore and R. Smith, *Philos. Mag. A* **74**, 1439 (1996).
  - <sup>48</sup>G.C. Abell, *Phys. Rev. B* **31**, 6184 (1985).
  - <sup>49</sup>J. Tersoff, *Phys. Rev. B* **37**, 6991 (1988).
  - <sup>50</sup>J. Tersoff, *Phys. Rev. Lett.* **61**, 2879 (1988).
  - <sup>51</sup>K. Nordlund, J. Keinonen, and T. Mattila, *Phys. Rev. Lett.* **77**, 699 (1996).
  - <sup>52</sup>J. Tersoff, *Phys. Rev. B* **39**, 5566 (1989).
  - <sup>53</sup>M.V.R. Murty and H.A. Atwater, *Phys. Rev. B* **51**, 4889 (1995).
  - <sup>54</sup>H.U. Jäger and M. Weiler, *Diamond Relat. Mater.* **7**, 858 (1998).
  - <sup>55</sup>W. Zhu, Z. Pan, Y. Ho, and Z. Man, *Nucl. Instrum. Methods Phys. Res. B* **153**, 213 (1999).
  - <sup>56</sup>R. Smith and K. Beardmore, *Thin Solid Films* **272**, 255 (1996).
  - <sup>57</sup>H.U. Jäger and K. Albe, *J. Appl. Phys.* **88**, 1129 (2000).
  - <sup>58</sup>*CRC Handbook of Chemistry and Physics*, 76th ed., edited by D.R. Lide (CRC Press, Boca Raton, FL, 1995).
  - <sup>59</sup>J.P. Biersack and L.G. Haggmark, *Nucl. Instrum. Methods* **174**, 257 (1980).
  - <sup>60</sup>J.F. Ziegler (private communication).
  - <sup>61</sup>E. Vietzke, K. Flaskamp, V. Philipps, G. Esser, P. Wienhold, and J. Winter, *J. Nucl. Mater.* **145-147**, 443 (1987).
  - <sup>62</sup>A.F. Voter, *Phys. Rev. Lett.* **78**, 3908 (1997).
  - <sup>63</sup>A.F. Voter and M.R. Sorensen, in *Multiscale Modelling of Materials*, edited by V. V. Bulatov *et al.*, MRS Symposia Proceedings No. 538 (Materials Research Society, Pittsburgh, 1999), p. 427.
  - <sup>64</sup>S.J. Stuart, A.B. Tutein, and J.A. Harrison, *J. Chem. Phys.* **112**, 6472 (2000).
  - <sup>65</sup>E. Salonen, K. Nordlund, J. Keinonen, and C. H. Wu (unpublished).